Version of Record: https://www.sciencedirect.com/science/article/pii/S0951832022003362
Manuscript_70f21915842e92d9385785683b71b633

Physics-Informed Machine Learning Assisted Uncertainty Quantification for the Corrosion of Dissimilar Material Joints

Parth Bansal[a], Zhuoyuan Zheng[a], Chenhui Shao[b], Jingjing Li[c], Mihaela Banu[d], Blair E Carlson[e], Yumeng Li[a,†]

[†] Corresponding author, yumengl@illinois.edu

[a] *Department of Industrial and Enterprise Systems Engineering, University of Illinois at Urbana-Champaign, Urbana, IL 61801*

[b] *Department of Mechanical Science and Engineering, University of Illinois at Urbana- Champaign, Urbana, IL 61801*

[c] *Department of Industrial and Manufacturing Engineering, The Pennsylvania State University, University Park, PA 16802, USA*

[d] *Department of Mechanical Engineering, University of Michigan, Ann Arbor, MI 48109, USA*

[e] *Manufacturing Systems Research Laboratory, Global Research and Development, General Motors LLC, Warren, MI 48092, USA*

***Abstract*- Jointing techniques like the Self-Piercing Riveting (SPR), Resistance Spot Welding (RSW) and Rivet-Weld (RW) joints are used for mass production of dissimilar material joints due to their high performance, short cycle time, and adaptability. However, the service life and safety usage of these joints can be largely impacted by the galvanic corrosion due to the difference in equilibrium potentials between the metals with the presence of electrolyte. In this paper, we focus on Al-Fe galvanic corrosion and develop physics-informed machine learning based surrogate model for statistical corrosion analysis, which enables the reliability analysis of dissimilar material joints under corrosion environment. In this study, a physics-based finite element (FE) corrosion model has been developed to simulate the galvanic corrosion between a Fe cathode and an Al anode. Geometric and environmental factors including crevice gap, roughness of anode, conductivity, and the temperature of the electrolyte are investigated. Further, a thorough Uncertainty Quantification (UQ) analysis is conducted for the overall corrosion behavior of the Fe-Al joints. It is found that the electrolyte conductivity has the largest effects on the material loss and needs to be managed closely for better corrosion control. This will help in designing and manufacturing joints with improved corrosion performance.**

I. Introduction

Self-Piercing Riveting (SPR), Resistance Spot Welding (RSW) and Rivet-Weld (RW) are some of the extensively used joining techniques in the automotive and other industrial fields [1-3]. These joints can be used for a variety of applications involving the joining of similar or dissimilar materials. The SPR joining technique is a mechanical joining process which is used to join two or more sheets of materials by creating a metallic interlock between them [4]. RSW process uses the resistance heat between sheet interfaces to create a localized fusion zone which upon cooling, forms a weld joint. The RW joining technique is a hybrid joining method which combines the strengths of both the SPR and RSW joining techniques while by-passing the weaknesses of both these methods.

During the applications of these joining methods for dissimilar metals such as steel and aluminum, the joints can be susceptible to galvanic corrosion in the presence of an electrolyte [5]. When the two dissimilar metals are being joined, crevices and gaps form among the metal sheets and the rivets, which can sometimes act as the nucleation sites for the galvanic corrosion [6]. As a result, the corrosion induced material loss and geometry change of the joints can cause performance degradation, which plays an important role in the failure and fatigue of the joints and therefore reduces their useful life. Other corrosion related phenomena such as the formation of the corrosion products can also lead to problems by covering the surface of the metals. This can change the geometry of the joint and therefore impact the internal loading of the joint, leading to unexpected stress concentrations in the joint and other damages [7, 8]. Experimental studies on other kinds of dissimilar material joints such as magnetic pulse welding (MPW) joints have also been conducted [9]. A difference is found in the failure mechanism of the two pairs of joints that are tested due to the presence of zinc in one of the tested specimens. It is seen that the

existence of zinc layer can lead to the reduction in the total electrochemical corrosion rate of aluminum/steel joints, but it also resulted in the reduction in the strength of the weld, thus leading to different failure mechanisms. Various studies have been performed to study the nucleation, initiation and propagation of localized corrosion and the corrosion protection of such joints [10-12]. Kotadia et al. [13] conducted experimental studies on the performance of dissimilar metal SPR joints and coatings. They found that corrosion had significantly influenced the lap shear performance and the failure mechanism of the joints and these results were dependent upon the type of coating on the joints. The microstructure evolution of corroded SPR and RSW Al-Fe joints were studied by Wen et al. [14] and they found that there is a difference in the corrosion process in these joints due to the formation of secondary phase precipitate because of the heat generated during welding. Additionally, the corrosion behavior in Aluminum alloy and galvanized steel RSW and SPR joints were investigated in salt spray environment [15], and it was reported that the crevice generated by different joining methods has an important impact on corrosion behavior. The significant impact of the uncertainties associated with the geometric and environmental factors as well as the joining methods on the corrosion behaviors, as reported in the literature, necessitates the uncertainty quantification (UQ) studies for the corrosion of dissimilar material joints.

Numerical methods, e.g., finite element (FE) modeling, are powerful tools which are used to investigate the effect of different geometrical and environmental factors on the corrosion initiation and evolution, which can be challenging to study using experimental testing, and quantitatively characterize the corrosion phenomena. Dependences of corrosion on various variables, e.g., the geometry of the metals, pH value of the electrolyte bath, etc., have been studied using the numerical methods [16, 17]. For example, Wang et al. [18] investigated the effect of initial pit size, corrosion pitting current, and material properties on the fatigue life of corrosion aircraft materials by creating a probabilistic model based on a quantitative evaluation of the nucleation and growth of pits and crack propagation processes. Stochastic models, which incorporate the influence of stresses, relative humidity, pH and temperature, and can be used to characterize both corrosion volume and depth growth have also been developed [19]. Xie et al. [20] conducted multi-state Markov modeling of pitting corrosion in stainless steel which was exposed to chloride-containing environment. Numerical simulation work studying the dependence on pH on galvanic corrosion has been studied by Kamble et al. [21]. They used COMSOL models to conduct this study and found that increasing the pH causes a reduction in the corrosion rate. Shariati et al. [22] developed a novel approach to tackle the challenges seen in corrosion simulations by proposing a toolchain which is flexible, efficient and extensible. They use an algebraic flux correction method to solve the Poisson-Nernst-Planck model using parallel implementation that results in reduction of the simulation time by a factor of 4. A hybrid physics-based finite element model was developed to simulate the corrosion process of Fe-Al joints [23], where experimental results were used in the form of stochastic nucleation input information along with a physics-based FE model to simulate the corrosion in the SPR joints. These studies advance our knowledge regarding the corrosion phenomena and critical determining factors but lack the capability to quantitatively demonstrate the impact of corrosion on the overall performance of structures.

While employing physics-based FE simulations for UQ could result in prohibitively high computational costs, studies associated with the analysis of failure behaviors using data-driven machine learning as surrogate models have also been reported in the literature to improve the efficiency for UQ [24, 25]. Similarly, Stern et al. [26] used a machine learning based surrogate model to conduct accelerated Monte Carlo (MC) system reliability analysis with a good balance on the accuracy and computational efficiency. Similar machine learning based UQ studies have also been reported for other applications [27-29]. While the surrogate modeling approaches have been used for UQ studies, the performance of a surrogate model also depends on the dataset available for the model development. More data points in general lead to better model accuracy, they could however induce higher sampling costs since more function evaluations are required to acquire those data points. Consequently, adaptive sampling strategies [30-35] have been developed to improve the fidelity of the surrogate model using a minimum number of data points. By using adaptive sampling, an initial low fidelity surrogate model is often constructed firstly based on a small set of training samples, and additional sample points are identified iteratively, following

a certain sampling criterion, and added to the training data set to improve the performance of the surrogate model. Jones et al. developed an active learning method using an expected improvement measure based upon the response surface approach [30]. An efficient global reliability analysis (EGRA) method was developed by Bichon et al. [31] for structural systems design where an adaptive sampling criterion was created to balance the effort between a regional search near the response surface and a global search in the parametric space for reliability analysis. Lee and Jung [32] developed a constraint boundary sampling (CBS) method for constraint optimization problems, which focused on the approximation of constraint boundaries in the global design region using surrogate models. Echard et al. [33] developed an adaptive sampling strategy for reliability analysis where an active learning reliability method was combined with the adaptive Kriging and Monte Carlo simulation, namely the AK-MCS method. The AK-MCS method appears to be efficient for reliability analysis, since it is a local sampling approach and focuses only on a set of Monte Carlo samples generated from a given design point instead of approximating the performance function in the entire sample space. Wang and Wang [34] introduced a maximum confidence enhancement (MCE) based sequential sampling approach that can be employed simultaneously with the design optimization process, which uses the cumulative confidence level (CCL) as a sampling criterion to select sample points with the maximum value of the estimated CCL improvement successively. To address the issues related to sampling from data pools with different level of information fidelity levels, adaptive sampling strategies have been developed recently to considering adaptive surrogate modeling with partially observed information [35].

The machine learning based techniques have also been used for reliability assessment which focusses on corrosion effects. Dong et al. [36] studied the reliability of wind turbines considering the effect of corrosion and inspection. They quantified the effect of inspection, based on its quality for a given inspection strategy with and without the consideration of corrosion using probabilistic methods. An evidence theory-based kriging model was developed by Xie et al. [37] which used adaptive sampling to perform quantification of margins and uncertainties for the assessment of structural reliability for pressure vessels with corrosion damage. A time-dependent reliability-based redundancy assessment of corrosion effected deteriorated reinforced concrete structures against progressive collapse was presented by Feng et al. [38], where the modelling uncertainty was empirically specified. Ma et al. [39] developed a systematic framework to quantify hybrid uncertainties for the probabilistic prediction of corrosion damage in aging RC bridges which can concurrently tackle empirical information, sparse data and probability distribution with parameter uncertainty. A novel population-based pitting corrosion degradation model for piggable oil and gas pipelines is developed by Heidary et al. [40. They developed a hierarchical Bayesian model based on a non-homogeneous gamma process to combine the uncertain in-line inspection data and physics of failure knowledge of pitting corrosion process, which shows a good agreement with commonly used degradation models. Sarkar et al [41] present a stochastic reduced order model approach for quantifying uncertainty in systems undergoing corrosion. While considering the randomness in anode-cathode sizes, they use this model to estimate the statistics of corrosion current density and also compare the performance of this model against the more common Monte-Carlo approach. UQ is crucial role in reduction of uncertainties in the design and operation of structures under the influence of corrosion. However, a lot of the performed studies use Monte Carlo simulations to conduct uncertainty analysis, which can be computationally expensive, where our model integrates adaptive surrogate modeling with physics-based FE simulation platform which balance the conflict of computational expense and analysis fidelity in UQ.

In this study, a physics-informed machine learning approach has been developed to conduct UQ study on the galvanic corrosion process in the Fe-Al joints. A physics-based FE model is firstly developed and validated with the experimental results, which is used to simulate the galvanic corrosion process. This physics-based computational model forms the basis of the following parametric study wherein the influences of various geometric and environmental factors on the corrosion process and material loss are investigated. These factors include the gap between the electrodes, roughness of the anode and the temperature and conductivity of the electrolyte. Based on the material loss estimation, sensitivity analysis on the couplings of these factors is carried out to identify the main sources of uncertainty. To improve the

computational efficiency, a probabilistic confidence-based adaptive sampling technique is integrated with the physics-based simulation to study the impact of the synergetic effects between different uncertainty parameters. The adaptive sampling technique, which enables the cost-effective identification of multiple disjointed parametric regions with a minimum number of sample tests and verification efforts, helps in reducing the burden on running expensive corrosion simulations therefore improving the efficiency. Material loss is found for these synergistically coupled models, which then acts as the training data for the machine learning based surrogate model. The trained machine learning model can then be used to quantify the sources of uncertainty in the whole process and also to perform statistical corrosion analysis for Fe-Al joints, which will help the design and manufacturing of the Fe-Al joints with better corrosion performance.

II. Physics-informed Machine Learning Method for Uncertainty Quantification

In this section, the physics-informed machine learning method for uncertainty quantification is introduced. Section 2.1 explains the multiphysics-based corrosion modeling, and section 2.2 then details the physics-informed adaptive surrogate modeling technique employing the multiphysics-based simulation and Gaussian process adaptive sampling.

2.1 Multiphysics-based Corrosion Modeling

The physics-based FE model is developed to simulate the corrosion process, which is implemented in the COMSOL Multiphysics Software. This model takes into consideration the mass transport of O_2 and other ionic species (i.e. Al^{3+}, Na^{+}, Ca^{2+}, OH^{-}, Cl^{-}) in the electrolyte, the local kinetic electrochemical reactions, as well as the dynamic dissolution of the Al anode. This FE model consists of two main modules: the secondary current distribution module and the transport of diluted species module. The secondary current distribution module is used to simulate the electrochemical reactions on the surface of the Fe and Al electrodes, whereas the transport of diluted species module is used to simulate both diffusion and migration terms of the mass transport for all the different ionic species.

The kinetic simulations of the electrochemical reactions are conducted using the secondary current distribution module. The cathodic reaction on the Fe rivet surface (Eq. 1) and the local anodic dissolution of Al from the anode (Eq. 2) are simulated in this module. The corrosion process occurs at an open-circuit potential and is driven by the galvanic effect. There is no external polarization that will affect this process.

$$O_2 + 2H_20 + 4e^- \rightarrow 4OH^- \tag{1}$$

$$Al \rightarrow Al^{3+} + 3e^- \tag{2}$$

Mass transportations of the different ionic species are predicted using the transport of diluted species module via the Nernst-Planck equations. The concentration changes of all the involved species are calculated using the combination of the mass conservation (Eq. 3) and the electro-neutrality equation (Eq. 4) whereas the mobility of the different involved species of ions is calculated using the Nernst-Einstein equation (Eq. 5). The summation in Eq. (4) is done through varying i for the different ionic species that are involved in the reactions.

$$\partial C_i/\partial t = -\nabla(-D_i\nabla C_i + C_i u - Z_i m_i F C_i \nabla\phi_l) \tag{3}$$

$$\sum Z_i C_i = 0 \tag{4}$$

$$m_i = D_i/RT \tag{5}$$

where, C_i, D_i, Z_i and m_i are the concentration, diffusion coefficient, charge number and mobility of

species i , respectively. F is the Faraday constant, t denotes the time, and ϕ_l is the electric potential of the electrolyte. T denotes the temperature of the electrolyte and R is the universal gas constant. The potential gradient $\nabla\phi_l$ term is used to calculate the electrolytical potential driven migration of ionic species. The flow velocity u of the electrolyte is always equal to 0 since a stagnant condition of the electrolyte is assumed. To simulate the effect of constantly replenishing electrolyte, the edges of the domain have been assigned a constant value for the OH^-, Na^+, Ca^{2+} and Cl^- ions.

The transport of dilutes species (Eq. 6) is used to describe the ionic current density in the electrolyte, which consists of both the diffusion and the migration terms. And the current density i_l is obtained by solving the equation of charge conversation (Eq. 7).

$$i_l = F\sum_{i=1}^{n} Z_i\,(-D_i\nabla C_i + C_i u - Z_i m_i F C_i \nabla\phi_l) \tag{6}$$

$$\nabla i_l = 0 \tag{7}$$

An Arbitrary Lagrangian-Eulerian Formulation (ALE) method with free deformation is used to trace the corrosion front boundary of the Al sheet, i.e., the moving boundary of the domain. This method allows the computational mesh inside the domain to move arbitrarily, in order to optimize the shapes of the elements. Meanwhile, the mesh on the boundaries and the interfaces of the domains can move along with the material which helps in precisely tracking these boundaries and interfaces as the simulation proceeds. This ALE method is able to capture a bigger and a more precise level of deformation as compared to other methods by allowing the boundaries to move without the need for the mesh's movement to follow the material [42].

To simulate the galvanic corrosion in dissimilar material joints like RSW, SPR and RW as shown in Figure 1, a simple FE model is adopted to include an Al anode, a Fe cathode and a gap filled with electrolyte. This model has the Al anode on the bottom and the Fe cathode on the top. These electrodes are separated by a gap, which is filled with electrolyte. A schematic description of this model is given in Figure 2, with the highlighted boundary acting as the corrosion initiation site on the anode.

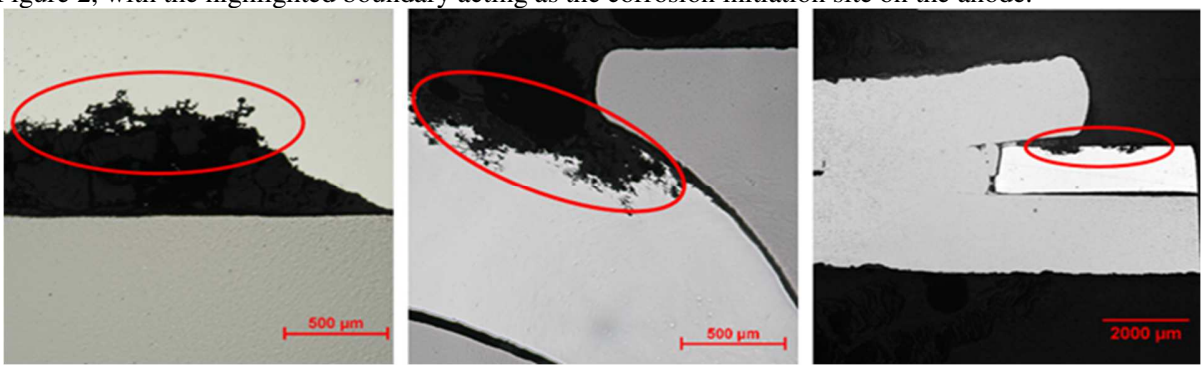

FIGURE 1: GALVANIC CORROSION HIGHLIGHTED (IN RED) IN RSW, SPR AND RW JOINTS RESPECTIVELY

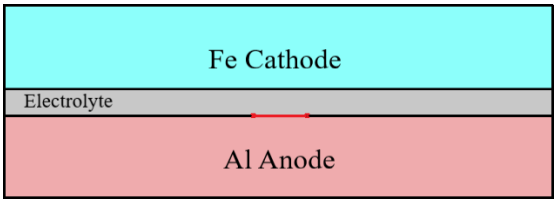

FIGURE 2: SIMULATION MODEL SETUP SHOWING THE Fe CATHODE (BLUE), THE Al ANODE (RED) AND THE ELECTROLYTE (GREY)

Using the FE model in Figure 2, four main geometric and environmental couplings, namely the gap between the electrodes, the roughness of the anode and conductivity and temperature of the electrolyte, which effect the corrosion process and the material loss during galvanic corrosion have been identified [15, 16, 44-46]. Material loss in terms of area loss or weight loss can be used to understand the failure due to corrosion by looking at the effect it has on the joint properties or the corrosion rate [47-49]. The implementation of all the investigated parameters is shown in Figure 3, whereas the investigated ranges for these parameters are given in Table 1. Ranges of parameters such as the crevice gap and roughness of the anode have been selected based on analyzing the experimental work [14, 15] on experimental corrosion testing on dissimilar material joints.

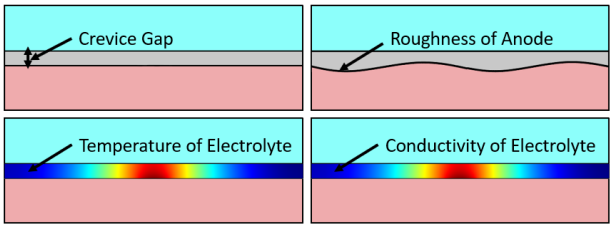

FIGURE 3: IMPLEMENTATION OF THE DIFFERENT GEOMETRIC AND ENVIRONMENTAL COUPLINGS IN COMSOL

TABLE 1: INPUT PARAMETER RANGES

Input Parameter	Range
Crevice Gap (mm)	0.0050 – 0.0075
Roughness of Anode (μm)	0 – 1
Temperature of Electrolyte (K)	273.15 – 293.15
Conductivity of Electrolyte (S/m)	0.5 – 1.0

Based on the material loss calculations for varying an individual environmental and geometric parameter, sensitivity analysis is conducted to understand how the different parameters effect material loss and to see which parameters play a major role in impacting the corrosion process. A normalized sensitivity (σ) is calculated for each parameter based on Eq. (8):

$$\sigma = \left\langle \frac{[k_i(q_i + \Delta q_i) - k_i(q_i)]/\bar{k}_i}{\Delta\, q_i/\bar{q}_i} \right\rangle \tag{8}$$

where, $\overline{q_i}$ is the value of the i^{th} operation parameter in the baseline design, $\overline{k_i}$ is the calculated property variation with respect to the i^{th} operation parameter, and Δq_i is the difference of the parameter. Using this above equation, the sensitivity value is calculated for each parameter and only those parameters which have a high sensitivity value to variations are thought to be key influencing factors affecting the material loss and hence the uncertainty quantification on these identified factors in the corrosion process would be conducted. Results from this sensitivity analysis are given in the Section 3.1. Once the key influence factors are identified, we then move onto quantifying the sources of uncertainty and their impacts on the corrosion performances using the physics-informed adaptive surrogate models.

2.2 Physics-Informed Adaptive Surrogate Modeling

For UQ analysis regarding corrosion, techniques such as the Monte Carlo simulation methods can be prohibitively expensive due to high computational costs associating with physics-based simulations. Considering the large parameter space in corrosion analysis, we employ machine learning (ML) techniques in order to reduce the overall computational costs of UQ analysis for the corrosion of

dissimilar material joints.

In this study, a gaussian process (GP) surrogate model is adopted since this model performs better as compared to simple polynomial fitting models on non-linear functions. A Gaussian process is a collection of random variables, any finite number of which have a joint Gaussian distribution. Gaussian process model is an extension of the standard linear regression model where the linear form of the standard model is replaced by a random process. This GP model is defined using two parameters as shown in Eq. (9).

$$f(x) \sim GP(m(x), k(x, x')) \tag{9}$$

where, $m(x)$ is the mean and $k(x, x')$ is the covariance function which defines the correlation of any two sample points x and x'. In this model, it is also assumed that the correlation between errors is related to the distance between the corresponding points. We use a Squared-Exponential (SE) kernel (Eq. 10) as the covariance function in our model. This kernel uses the Euclidean distance measure to show similarity between the sample points.

$$k(x, x') = \sigma^2 \exp\left(-\frac{1}{2l}(x - x')^2\right) \tag{10}$$

where, σ denotes the vertical scale which describes how much span the function has vertically and l denotes the horizontal scale which describes how quickly the correlation between two points drops as the distance between them increases. So, a higher l results in a smooth function whereas a lower l results in a wiggly function. Another reason to choose a GP machine learning model is that the prediction is probabilistic so that one can compute empirical confidence intervals and decide based on those if one should refit (online fitting, adaptive fitting) the prediction in some region of interest. Therefore, using this method greatly reduces the overall number of iterations required in order to map a multi-input system with a large number of design points. The training data for the model is generated based on the random configurations of the environmental and geometric factors within their ranges. However, the training process for the ML surrogate model by itself is still computationally expensive, and hence in this study a probabilistic confidence-based based adaptive sampling (PCAS) scheme [34, 51] is adopted for the sequential updating of the GP models to further reduce these costs.

With an initial set of sample points $\mathbf{X}_E$ and system responses $\mathbf{Y}_E$, a GP model, $g(.)$, can be constructed accordingly. However, this GP model usually has a low fidelity, and thus needs to be updated. The principal idea of PCAS is to adaptively evaluate the uncertain parametric space based on the feedbacks from sample points in a sequential manner. The prediction of the response (e.g. material loss due to corrosion) at point $\mathbf{x}_i$ from a GP model can be considered as a random variable that follows the Gaussian distribution. For any given sample point $\mathbf{x}_i$, based on the GP model prediction of its response, $g(\mathbf{x}_i)$, it can be accordingly classified as a sampling point in the failure region or safe region, by comparing with a threshold value g_0. With this classification, all Monte Carlo sample points can be accordingly categorized into two classes, the failure class and the safe class, where the failure class includes all sample points at which the predicted responses $g(\mathbf{x}_i) - g_0 > 0$, and the safe class at which $g(\mathbf{x}_i) - g_0 \leq 0$. Knowing that the GP prediction can be considered as a random variable, thus the classification of sample point becomes probabilistic. Here we define the probability of having a correct classification of a sample point as the classification confidence value (CCV). To compute the CCV, the sample points at two difference classes must be treated differently. For sample points in the failure class, since failure is defined as $g(\mathbf{x}_i)$-$g_0 > 0$, the CCV value indicates the probability that the sample point is at the failure region, which can be accordingly calculated as the area of the normal cumulative distribution function in the interval of $(0, \infty)$ as

$$\mathrm{CCV}(\mathbf{x}_i) = \begin{cases} \dfrac{1}{\sqrt{2\pi \cdot e(\mathbf{x}_i)}} \displaystyle\int_0^{\infty} e^{-\frac{1}{2}\frac{[y-g(\mathbf{x}_i)]^2}{e(\mathbf{x}_i)}} dy & \text{for all } i \text{ where } g(\mathbf{x}_i) - g_0 > 0 \\ \dfrac{1}{\sqrt{2\pi \cdot e(\mathbf{x}_i)}} \displaystyle\int_{-\infty}^{0} e^{-\frac{1}{2}\frac{[y-g(\mathbf{x}_i)]^2}{e(\mathbf{x}_i)}} dy, & \text{for all } i \text{ where } g(\mathbf{x}_i) - g_0 \le 0 \end{cases} \tag{11}$$

where $g(\mathbf{x}_i)$ and $e(\mathbf{x}_i)$ are the predicted response at the point $\mathbf{x}_i$ and its variance of the prediction, respectively. Similarly, for sample points in the safe class, the CCV value indicates the probability that the sample point is at the safe region, which can be accordingly calculated as the area of the normal cumulative distribution function in the interval of $(-\infty, 0)$. Based upon the definition, the CCV should be a positive value within (0.5, 1), with a higher value indicates higher classification confidence. Considering both failure and safe regions, the CCV of the sample point $\mathbf{x}_i$ can be generally calculated as

$$\mathrm{CCV}(\mathbf{x}_i) = \Phi\left(\frac{|g(\mathbf{x}_i)|}{\sqrt{e(\mathbf{x}_i)}}\right), \quad i = 1, 2, \ldots, n \tag{12}$$

where Φ is standard normal cumulative distribution function, $|.|$ is the absolute operator, n is the total number of Monte Carlo samples, and $g(\mathbf{x}_i)$ and $e(\mathbf{x}_i)$ are the predicted response at the sample point $\mathbf{x}_i$ and the variance of this prediction, respectively. These values can be obtained directly from the constructed GP model at the current sampling iteration. By using Eq. (12), failure potentials of the Monte Carlo samples can be calculated based on their GP predicted means and the variance of the responses.

In order to improve the fidelity of the GP model using the multiphysics-based corrosion FE simulations, simulation sample points must be accordingly chosen from different regions during the adaptive sampling process, as those samples points could bring much information about the performance function at particular regions and thus are more valuable. Therefore, in the PCAS approach, the sample point will be selected based upon a sampling rule of improving the classification confidence values using the GP model, thus the sample point with the minimum CCV, $\mathbf{x}^*$, will be selected in each GP model updating iteration, and the corresponding performance value $\mathbf{y}^*$ will be evaluated. This selected sample $\mathbf{x}^*$ with its actual response value $\mathbf{y}^*$ are then added into $\mathbf{X}_E$ and $\mathbf{Y}_E$ respectively, and the GP model will be accordingly updated with new sample points added. The updated GP model is then used to predict the responses of Monte Carlo samples again. This search and update process works iteratively, and it is terminated when the minimum CCV value reaches a predefined threshold, CCV_t. This stopping rule is defined as

$$\min \quad CCV_i \ge CCV_t, \quad i = 1, 2, \ldots, n \tag{13}$$

where CCV_i is the CCV value for the sample point $\mathbf{x}_i$, and CCV_t is the predefined CCV threshold. As $\mathrm{CCV_t}$ represents the confidence on the prediction of the surrogate model, the higher the $\mathrm{CCV_t}$, the better prediction accuracy for the surrogate model. The $\mathrm{CCV_t}$ should be determined based upon specific applications, and a value between [0.95, 1) is generally desirable to ensure a good balance of accuracy and efficiency, and in this study 0.95 has been used for the CCV_t.

A flowchart describing the complete process of the adaptive surrogate modeling using the PCAS technique is given in Figure 4. The process starts (Step 1) with the generation of the sampling population $\mathbf{S}$. In this study, $\mathrm{N_{grid}}$ number of grid samples in the input parameter space are generated. Then the process moves onto the initial Design of Experiment (DOE), which generates an initial set of N_I sample points $\mathbf{X}_E$ and their corrosion material loss responses $\mathbf{Y}_E$ evaluated using the multiphysics-based FE simulations (Step 2). In the next step (Step 3), an initial GP model is developed with ($\mathbf{X}_E$, $\mathbf{Y}_E$). This initial GP model is then used to predict the material loss $\mathbf{g}$ for the samples in the sampling population $\mathbf{S}$ (Step 4). By using the PCAS sampling criteria, the next sample point, $\mathbf{x}^*$, is found in $\mathbf{S}$ (Step 5). Now, the stopping condition is checked (Step 6), and if it isn't fulfilled then the identified sample point, $\mathbf{x}^*$, is evaluated using multiphysics-based FE simulation to obtain the corrosion material loss, y* (Step 7). By including the new sample point ($\mathbf{x}^*$, y*) into the training data ($\mathbf{X}_E$, $\mathbf{Y}_E$), the GP model can be updated, and with the updated GP model, the PCAS sampling process can be continued.

Steps 3-7 are repeated until the stopping criteria in Step 6 is fulfilled at which point, we get a robust GP surrogate model which is ready to be used to conduct the UQ in the design space.

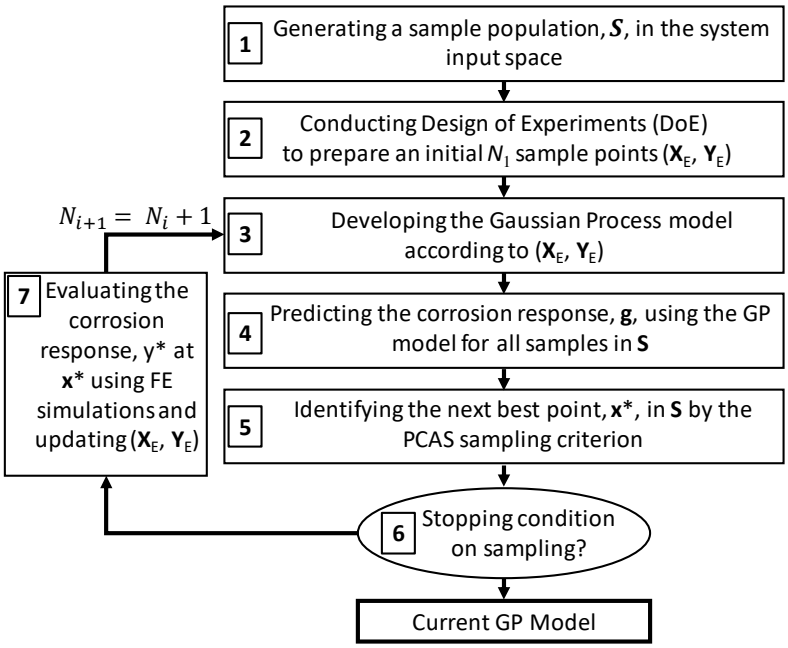

FIGURE 4: PROCESS FLOWCHART of ADAPTIVE SURROGATE MODELING USING THE PCAS

III. Uncertainty Quantification Results and Discussion

3.1 Corrosion Propagation and Parametric Study

To demonstrate the proposed platform for statistical corrosion analysis, corrosion is simulated based on the developed FE model for a period of 3600 seconds. Figure 5 shows the electrolytical potential in the electrolyte with the anode (light grey), the cathode (dark grey) and the electrolyte (rainbow colored part). Comparing Figure 5 with Figure 2 shows how the corrosion process results in the material loss and how this corrosion front propagates. The material loss for the FE model is then calculated using the 2D surface integration function in COMSOL to quantify the corrosion performance. The total area covered by the electrolyte domain is noted at both the beginning and the end of the simulation and then the initial value is subtracted from latter value to get the material loss. The evaluated material loss is needed for the corrosion analysis as we can use it to understand how the mechanical properties and joint performance changes with changing material loss.

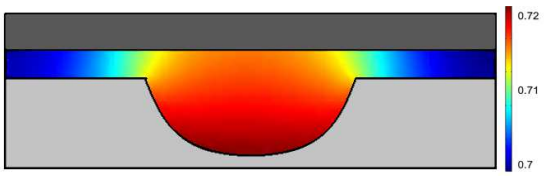

FIGURE 5: SIMULATED CORROSION AT 3600s FOR THE SIMPLE MODEL

FE simulations were carried on the identified geometric and environmental couplings and material loss due to corrosion was found. Figure 6 shows the material loss trends for the four parameter factors. It

is observed that as the material loss increases with increasing roughness of the anode, conductivity, and temperature of the electrolyte whereas the material loss decreases as the crevice gap between the anode and the cathode increases. Increasing the crevice distance leads to the increase of internal resistance in electrolyte and reduction of current density (corrosion rate) on the anode surfaces, thereby decreasing the material loss. The increase in roughness leads to more material loss as it has been observed that rougher surfaces lead to more corrosion initiation sites and hence more corrosion. The increased corrosion due to increasing temperature can be attributed to the increase in the diffusion rate of ions in the electrolyte because of higher temperatures and finally corrosion decreases with decreasing conductivity due to less ions being available for corrosion which results in decreased over-potentials and reduced reaction rates at the electrodes surfaces.

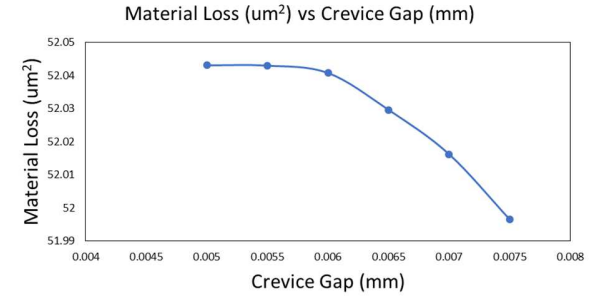

(a)

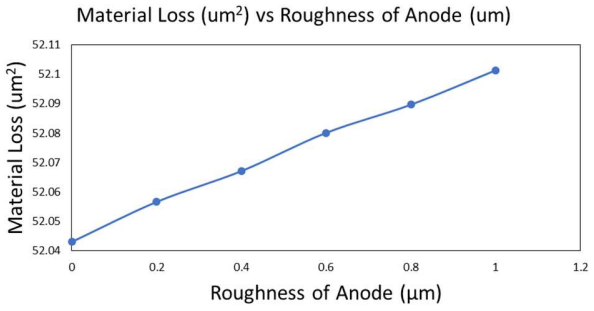

(b)

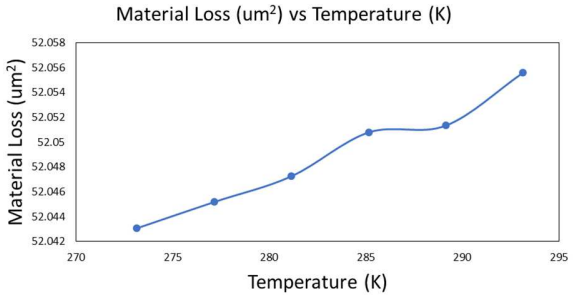

(c)

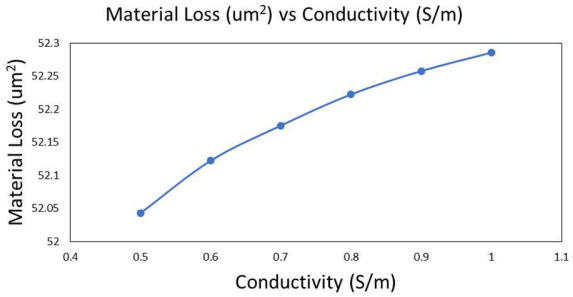

(d)

FIGURE 6: MATERIAL LOSS TRENDS FOR DIFFERENT GEOMETRIC AND ENVIRONMENTAL COUPLINGS

Based on the above seen material loss values and Eq. (8), a sensitivity analysis was conducted. The sensitivity values for the different parameters are given in Table 2.

TABLE 2: SENSITIVITY ANALYSIS

Input Parameter	Sensitivity Value
Crevice Gap (mm)	0.002233
Roughness of Anode (μm)	0.000559
Temperature of Electrolyte (K)	0.003409
Conductivity of Electrolyte (S/m)	0.006968

Based on this sensitivity analysis it is found that the crevice gap, conductivity, and temperature are the parameters to which the material loss is most sensitive. In addition, the conductivity of the electrolyte is found to be the parameter which effects the material loss the most and hence the conductivity of the electrolyte needs to be managed closely in order to better control the rate of corrosion. Therefore, in the uncertainty quantification study, only these three parameters, i.e. the crevice gap, conductivity and temperature, are considered as the input parameters for the FE and surrogate model.

TABLE 3: INITIAL FE SIMULATION RESULTS

Crevice Gap (mm)	Conductivity of Electrolyte (S/m)	Temperature of Electrolyte (K)	Material Loss (um^2)
0.0050	0.5	273.15	52.043
0.0050	1.0	283.15	52.285
0.0060	0.8	285.15	52.205
0.0070	0.7	289.15	52.132
0.0075	1.0	293.15	52.195
0.0055	0.6	277.15	52.121

3.2 GP based Surrogate Model Results

It is expensive to run the developed physics-based FE simulations over the whole parameter spaces. Therefore, to conduct UQ in an efficient manner, surrogate model was developed to replace the physics-based FE simulation. FE models were created for determined parameter sets to run corrosion simulations and generate training sampling dataset for developing GP based surrogate model. Care was taken to randomize the input parameters within the parameter spaces so as to get a spread-out initial training data set for the surrogate model. Table 3 shows these initial input parameter and material loss values. Staring with a small size of initial training samples, PCAS was used to identify critical sample locations in the

parameter spaces to be evaluated and added to the existing training sample, to adaptively enhance the fidelity of developed GP based surrogate model. This enables the development of high-fidelity surrogate model with minimized size of training dataset.

Based on PCAS sampling, corrosion simulations were carried out till the termination criteria was reached. For this study, the termination criterion for the surrogate model was that the relative error in material loss for a group of randomly selected points between the actual FE model and the surrogate model should be below $5\ x\ 10^{-4}$. To do this 20 random data points in the design space were selected and FE simulations were conducted for these points. After each sampling iteration wherein a new design point was added to the training data for the surrogate model, this model was used to predict the material loss at these 20 random points. Once the average relative error for these 20 points went below the defined value, the algorithm was terminated, and the surrogate model was believed to possess satisfying accuracy to replace the physics-based FE corrosion simulations for predicting the material loss in the defined parameter space. Figure 7a illustrates an example of the parameter space where all the parameter locations in the training dataset are shown in blue, the initial data points are shown in red and the ones determined by the PCAS sampling shown in green. The number of iterations and the history of relative error over the iterations is shown in Figure 7b.

Figure 7 shows several important aspects of this sampling process. Firstly, the whole design space is a 3-dimensional design space with a total data pool of 1331 available parameter points. Figure 7b shows that the actual number of sampling points that have been used in order to train a high-fidelity surrogate model is less 4% of the total design points. Therefore, by using PCAS sampling method to explore the different areas of the parameter space, the overall computational cost can be reduced drastically. Another important observation that can be seen from Figure 7b is that the relative error sometimes increases as more FE simulations are conducted. This is because the PCAS sampling approach moves from an explored area of sampling to an unexplored area for the new sampling point. While this movement improves the surrogate model locally in the critical regions, it may lead to relative error increases temporally on average considering the overall model. However, the accuracy of the surrogate model continues to decrease with more multiphysics-based simulation runs being acquired through the adaptive sampling process, which is evident in the presented results.

To validate the surrogate model, FE simulations were conducted on certain randomly chosen parameter points for which the material loss was also found using the surrogate model. These results along with the absolute percentage of error between the material loss values between the actual FE simulations and the surrogate model generated results are provided in Table 4. It can be observed that this absolute percentage error between the two methods is low, hence validating the developed surrogate model.

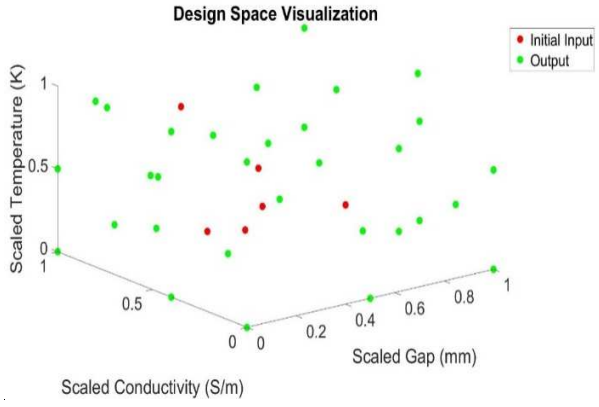

(a)

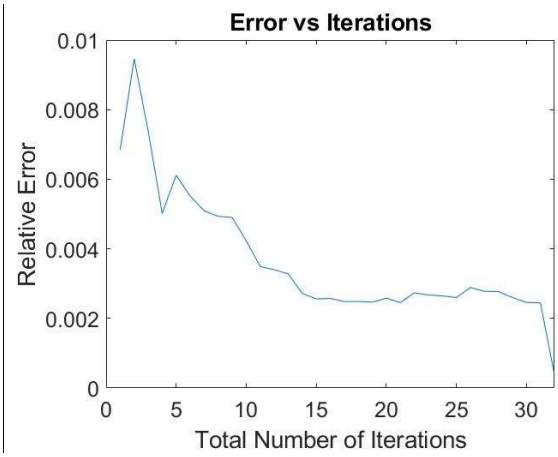

(b)

FIGURE 7: (a) VISUALIZED DESIGN SPACE: BLUE POINTS DENOTE ALL THE AVAILABLE DESIGN SPACE POINTS; RED POINTS DENOTE THE INITIAL INPUT POINTS AND THE GREEN POINTS DENOTE THE PCAS OUTPUT POINTS WHERE ACTUAL FE SIMULATIONS WERE CONDUCTED **(b)** PLOT FOR RELATIVE ERROR VS NUMBER OF REQUIRED ITERATIONS IN ORDER TO REACH THE TERMINATION CRITERIA

TABLE 4: COMPARISON BETWEEN FE SIMULATION AND GP SURROGATE MODEL RESULTS

Crevice Gap (mm)	Conductivity of Electrolyte (S/m)	Temperature of Electrolyte (K)	FE Material Loss (um^2)	GP Material Loss (um^2)	Absolute Error (%)
0.00625	0.60	277.15	52.10700	52.10727	5.29E-04
0.00725	0.80	281.15	52.15965	52.15990	4.88E-04
0.00675	0.95	273.15	52.22166	52.22180	2.69E-04
0.00525	0.65	289.15	52.15012	52.15152	2.70E-03
0.00575	0.85	287.15	52.22755	52.22729	5.02E-04

Finally, this developed high-fidelity surrogate model was used to generate the response surfaces of the material loss with respect to the three different input parameters as shown in Figure 8. These contour and response surface plots show the dependent and independent variable relationship. Figure 8a reveals that both gap and conductivity impact the material loss at a constant value of temperature. Figure 8b shows that for a steady value of gap, the material loss is mainly dependent on the conductivity of the electrolyte, whereas Figure 8c depicts that for a constant value of conductivity, the material loss is mainly influenced by the gap size with temperature influencing the material loss only at higher values.

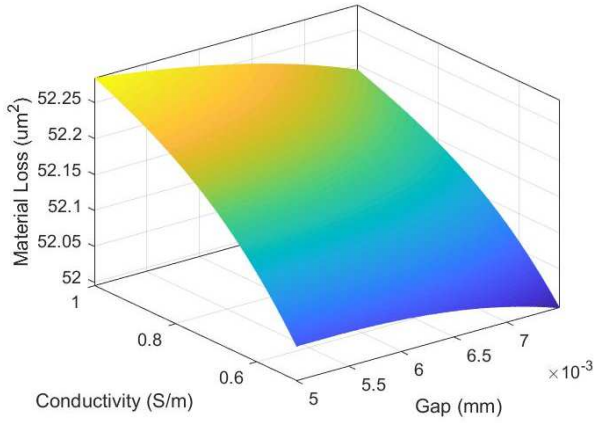

(a)

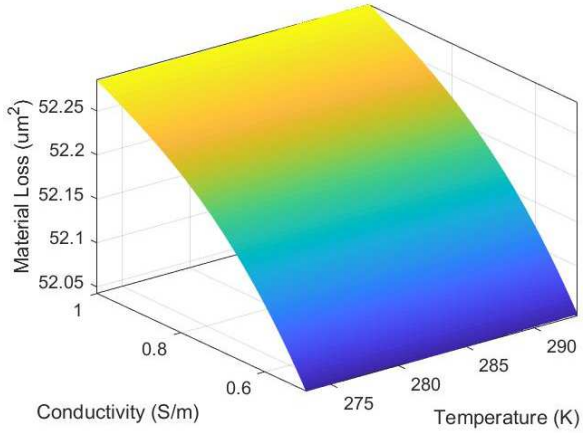

(b)

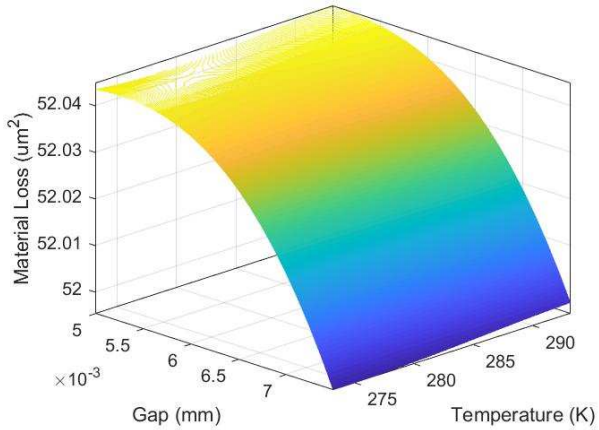

(c)

FIGURE 8: RESPONSE SURFACE FOR MATERIAL LOSS FOR DIFFERENT INPUT PARAMETERS: **(a)**

GAP vs CONDUCTIVITY vs MATERIAL LOSS **(b)** CONDUCTIVITY vs TEMPERATURE vs MATERIAL LOSS **(c)** TEMPERAURE vs GAP vs MATERIAL LOSS

3.3 Uncertainty Quantification Results

Once the surrogate model has been trained to accurately provide the material loss value in the parameter space, it can be used to conduct the uncertainty quantification study. In this study, the statistical distributions of the three uncertain input parameters have been assumed to be normally distributed, and the statistical information including the distribution type, mean and the standard deviation for each input parameters has been given in Table 5. With the information provided in Table 5, a total number of 10000 sample points have been randomly generated within the design space and used for the UQ study with the developed surrogate model. The histograms for these samples generated for these random parameters are shown in Figure 9. With the physics-informed surrogate models, the impacts of input parameters under given random distributions on the corrosion of the Al-Fe joints can be investigated and the distribution of the material loss under different cases can be determined, as discussed further below.

TABLE 5: UQ INPUT PARAMETER PROPERTIES

Input Parameter	Distribution	Mean	St. Dev.
Crevice Gap (mm)	Normal	6.25E-3	5E-4
Temperature of Electrolyte (K)	Normal	283	4.2
Conductivity of Electrolyte (S/m)	Normal	0.75	0.10

The histograms provided in Figure 10 show the results of the uncertainty quantification study for the material losses under different random input conditions, and the first four statistical moments, mean, standard deviation, skewness and kurtosis, for the material loss have been summarized in Table 6. As shown in Figure 10(a), the material loss shows the largest standard deviation when all three input parameters are considered random with the distribution information shown in Table 5. To explore the uncertainty impact of individual parameters, the corrosion material losses have also been provided by only considering one input parameter as random variable following a normal distribution while the other two are held constant at their mean values respectively, and the results have been shown in Figure 10(b)-(d) and also in Table 6. From the uncertainty quantification study results, it is interesting to see that (1) under all cases the mean value of the material loss has stayed relatively stable; (2) the electrolyte conductivity appears to have higher impact on the variability of the material loss, as compared to the crevice gap and temperature; (3) under all cases, the material loss appears to be negatively skewed; and (4) the variability of electrolyte temperature within the given range appears to have very limited impact corrosion material losses, as shown in Figure 10(d). This will help in designing and manufacturing joints with better corrosion performance.

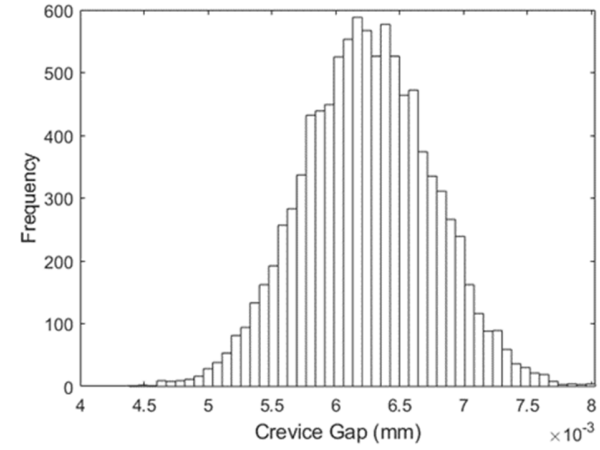

(a)

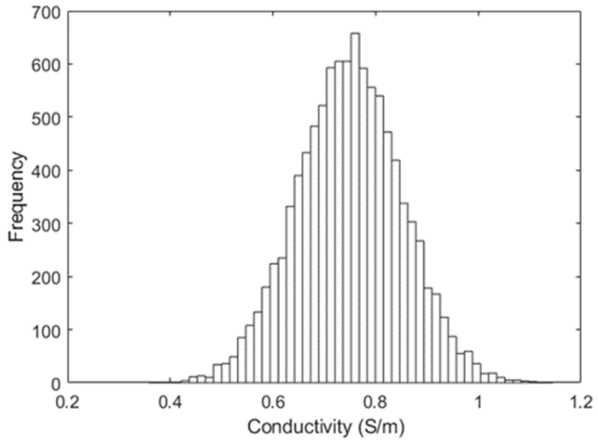

(b)

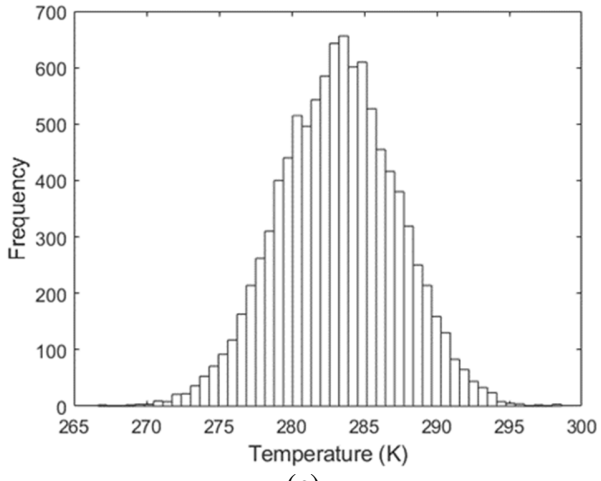

(c)

FIGURE 9: THE DISTRIBUTION OF THE THREE INPUT PARAMETERS: CREVICE GAP, ELECTROLYTE CONDUCTIVITY AND TEMPERATURE

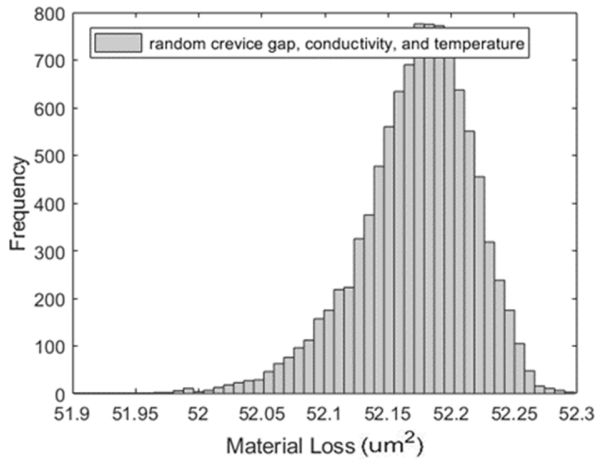
random crevice gap, conductivity, and temperature
Frequency
Material Loss (um^2)
800
700
600
500
400
300
200
100
0
51.9
51.95
52
52.05
52.1
52.15
52.2
52.25
52.3

(a)

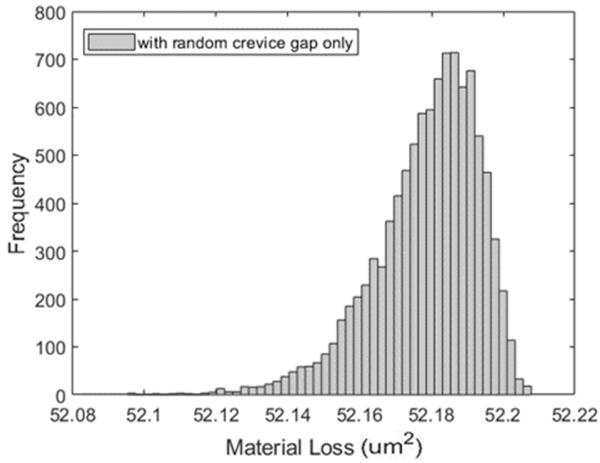
with random crevice gap only
Frequency
Material Loss (um^2)
800
700
600
500
400
300
200
100
0
52.08
52.1
52.12
52.14
52.16
52.18
52.2
52.22

(b)

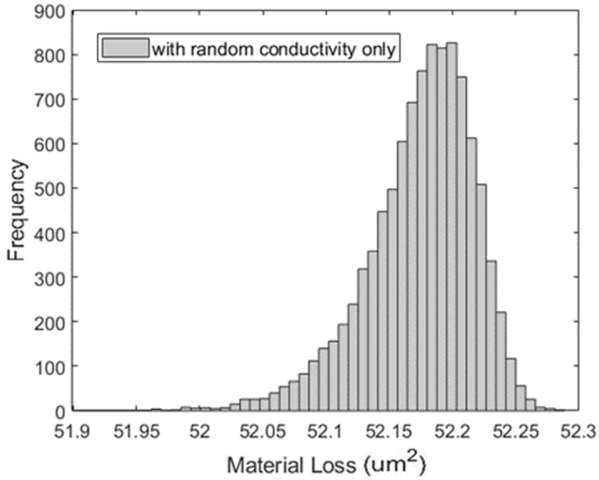
with random conductivity only
Frequency
Material Loss (um^2)
900
800
700
600
500
400
300
200
100
0
51.9
51.95
52
52.05
52.1
52.15
52.2
52.25
52.3

(c)

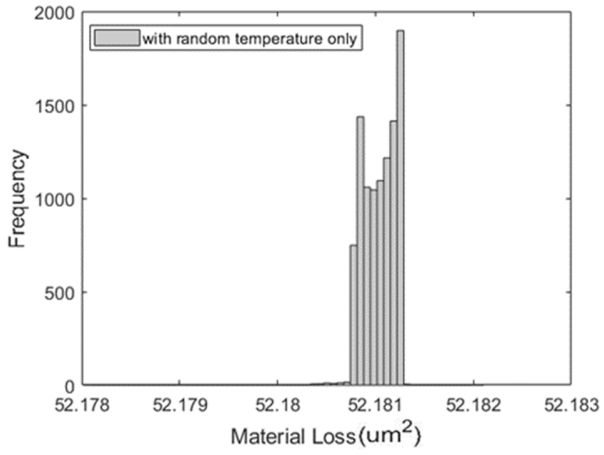

(d)

FIGURE 10: HISTOGRAM OF THE MATERIAL LOSS: (a) WITH RANDOM CREVICE GAP, CONDUCTIVITY AND TEMPERATURE, (b) WITH RANDOM CREVICE GAP ONLY, (c) WITH RANDOM CONDUCTIVITY ONLY, AND (c) WITH RANDOM TEMPERATURE ONLY

TABLE 6: UQ RESULTS FOR CORRISON MATERIAL LOSS WITH RANDOM INPUT PARAMETERS

Crevice Gap	Electrolyte Conductivity	Electrolyte Temperature	Material Loss (um^2)			
			mean	st. dev.	skewness	kurtosis
random	random	random	52.1722	0.0453	-0.7400	4.0455
random	constant	constant	52.1787	0.0147	-1.0300	4.6077
constant	random	constant	52.1746	0.0427	-0.9128	4.4195
constant	constant	random	52.1810	0.0002	-1.9017	26.0851

IV. Summary and Conclusion

In this study, uncertainty quantification was conducted on the galvanic corrosion of the dissimilar material joints between an aluminum anode and a steel cathode, using a physics-informed machine learning framework and the probabilistic confidence based adaptive sampling technique. An FE model was developed to simulate the corrosion evolution in the dissimilar material joints and estimate the resulted material loss. The sensitivity analysis were carried out based on the parametric study for different parameters including crevice gap, temperature and conductivity of the electrolyte and roughness of the anode. Based on this sensitivity analysis, crevice gap and the temperature and conductivity of the electrolyte were identified as the main parameters to which the material loss of the model was sensitive to.

A physics simulation informed machine learning based surrogate model was then developed in order to conduct uncertainty quantification on these parameters. The developed machine learning model employed a PCAS approach to map out the response surface over the entire parameter space by using a small number of sampling points, to conduct actual FE simulations on, in order to reduce the overall computational cost of the process and to improve its accuracy. The identified parameters, i.e. crevice gap, the temperature and conductivity of the electrolyte, and estimated material loss by the FE model for sampling points in the training dataset were used as the training data. Our results showed that the entire design space could be thoroughly scanned by using only around 4% of the overall available design points.

The distribution of the input parameters to the surrogate model was assumed to be normally distributed around the mean value of each parameter. This trained surrogate model was used to predict the material

loss output for the dataset which showed a slightly skewed distribution (with mean, standard deviation, skewness and kurtosis values equal to 52.173, 0.032, -0.471 and 0.238 respectively) of the material loss. The electrolyte conductivity appears to have higher impact on the variability of the material loss, as compared to the crevice gap and temperature. The developed framework based on physics-informed machine learning model is ready to be applied towards UQ analysis of the corrosion-induced material loss while considering various parameters, which can be used for the design and manufacturing of dissimilar material joints with satisfied corrosion performance.

Acknowledgement

This work was financially supported by the U. S. Department of Energy via Award No. DE-EE0008456.

References

[1] He, X., Pearson, I., & Young, K. (2008). Self-pierce riveting for sheet materials: state of the art. Journal of materials processing technology, 199(1-3), 27-36.

[2] Manladan, S. M., Abdullahi, I., & Hamza, M. F. (2015). A review on the application of resistance spot welding of automotive sheets. J. Eng. Technol, 10, 20-37.

[3] Hou, W.K., Wang, P.C. & Hu, S.J. (2007). Method of Joining Dissimilar Materials, US2005133483A.

[4] Li, D., Chrysanthou, A., Patel, I., & Williams, G. (2017). Self-piercing riveting-a review. The International Journal of Advanced Manufacturing Technology, 92(5), 1777-1824.

[5] Calabrese, L., Proverbio, E., Pollicino, E., Galtieri, G., & Borsellino, C. (2015). Effect of galvanic corrosion on durability of aluminium/steel self-piercing rivet joints. Corrosion Engineering, Science and Technology, 50(1), 10-17.

[6] Mandel, M., & Krüger, L. (2013). Determination of pitting sensitivity of the aluminium alloy EN AW-6060-T6 in a carbon-fibre reinforced plastic/aluminium rivet joint by finite element simulation of the galvanic corrosion process. Corrosion science, 73, 172-180.

[7] Bardal, E. (2007). Corrosion and protection. Springer Science & Business Media.

[8] Krüger, L., & Mandel, M. (2011). Electrochemical behaviour of aluminium/steel rivet joints. Corrosion science, 53(2), 624-629.

[9] Wang, S., Luo, K., Sun, T., Li, G., & Cui, J. (2021). Corrosion behavior and failure mechanism of electromagnetic pulse welded joints between galvanized steel and aluminum alloy sheets. Journal of Manufacturing Processes, 64, 937-947.

[10] Lim, Y.C., Squires, L., Pan, T.Y., Miles, M.P., Song, G., Wang, Y., & Feng, Z. (2015). Study of mechanical joint strength of aluminum alloy 7075-T6 and dual phase steel 980 welded by friction bit joining and weld-bonding under corrosion medium. Materials & Design, 69, 37-43.

[11] Maddela, S., & Carlson, B. E. (2019). Corrosion Characterization of Resistance Spot-Welded Aluminum and Steel Couple. Journal of Manufacturing Science and Engineering, 141(11), 111010.

[12] Yin, L., Jin, Y., Leygraf, C., Birbilis, N., & Pan, J. (2017). Numerical simulation of micro-galvanic corrosion in Al alloys: effect of geometric factors. Journal of the Electrochemical Society, 164(2), C75.

[13] Kotadia, H. R., Rahnama, A., Sohn, I. R., Kim, J., & Sridhar, S. (2019). Performance of dissimilar metal Self-Piercing Riveting (SPR) joint and coating behaviour under corrosive environment. Journal of Manufacturing Processes, 39, 259-270.

[14] Wen, W., Liu, T., Banu, M., Simmer, J., Carlson, B., & Hu, S.J. (2020). Corrosion Evolution in Al/Steel Dissimilar Joints. Proceedings of the ASME 2020 15th International Manufacturing Science and Engineering

Conference, 1, V001T02A005.

[15] Pan, B., Sun, H., Shang, S-L, Wen, W., Banu, M., Simmer, J.C., Carlson, B.E., Chen, N., Liu, Z-K, Zheng, Z., Wang, P., and Li, J., "Corrosion behavior in aluminum/galvanized steel resistance spot welds and self-piercing riveting joints in salt spray environment," Journal of Manufacturing Processes, vol. 70, pp. 608-620, 2021.

[16] Jia, J. X., Song, G., & Atrens, A. (2006). Influence of geometry on galvanic corrosion of AZ91D coupled to steel. Corrosion Science, 48(8), 2133-2153.

[17] Tsuyuki, C., Yamanaka, A., & Ogimoto, Y. (2018). Phase-field modeling for pH-dependent general and pitting corrosion of iron. Scientific reports, 8(1), 1-14.

[18] Chang, H. Y., Park, Y. S., & Hwang, W. S. (2000). Initiation modeling of crevice corrosion in 316L stainless steels. Journal of Materials Processing Technology, 103(2), 206-217.

[19] Wang, C., & Elsayed, E. A. (2020). Stochastic modeling of corrosion growth. Reliability Engineering & System Safety, 204, 107120.

[20] Xie, Y., Zhang, J., Aldemir, T., & Denning, R. (2018). Multi-state Markov modeling of pitting corrosion in stainless steel exposed to chloride-containing environment. Reliability Engineering & System Safety, 172, 239-248.

[21] Kamble, P. A., Deshpande, P. P., & Vagge, S. T. (2022). Numerical investigation of galvanic corrosion between galvanized steel and mild steel in bolted joint. Materials Today: Proceedings, 50, 1923-1929.

[22] Shariati, M., Weber, W. E., & Höche, D. (2022). Parallel simulation of the Poisson–Nernst–Planck corrosion model with an algebraic flux correction method. Finite Elements in Analysis and Design, 206, 103734.

[23] Zheng, Z., Bansal, P., Wang, P., Shao, C., & Li, Y. (2020). Corrosion Modeling and Prognosis of the Al-Fe Self-Pierce Riveting Joints. Proceedings of the ASME 2020 International Mechanical Engineering Congress and Exposition, 14, V014T14A017.

[24] Nannapaneni, S., Hu, Z. & Mahadevan, S. Uncertainty quantification in reliability estimation with limit state surrogates. *Struct Multidisc Optim* **54,** 1509–1526 (2016). https://doi.org/10.1007/s00158-016-1487-1

[25] Li, M., and Wang, Z., Surrogate model uncertainty quantification for reliability-based design optimization, Reliability Engineering & System Safety, 192, 2019, 106432. https://doi.org/10.1016/j.ress.2019.03.039.

[26] Stern, R. E., Song, J., & Work, D. B. (2017). Accelerated Monte Carlo system reliability analysis through machine-learning-based surrogate models of network connectivity. Reliability Engineering & System Safety, 164, 1-9.

[27] Rehme, M. F., Franzelin, F., & Pflüger, D. (2021). B-splines on sparse grids for surrogates in uncertainty quantification. Reliability Engineering & System Safety, 209, 107430.

[28] Jakeman, J. D., Kouri, D. P., & Huerta, J. G. (2022). Surrogate modeling for efficiently, accurately and conservatively estimating measures of risk. Reliability Engineering & System Safety, 108280.

[29] Y. Dong, A. P. Teixeira, and C. Guedes Soares, "Application of adaptive surrogate models in time-variant fatigue reliability assessment of welded joints with surface cracks," Reliability Engineering & System Safety, vol. 195, p. 106730, 2020, doi: https://doi.org/10.1016/j.ress.2019.106730.

[30] D. R. Jones, M. Schonlau, and W. J. Welch, "Efficient Global Optimization of Expensive Black-Box Functions," *Journal of Global Optimization*, vol. 13, no. 4, pp. 455–492, 1998, doi: 10.1023/A:1008306431147.

[31] B. J. Bichon, M. S. Eldred, L. P. Swiler, S. Mahadevan, and J. M. McFarland, "Efficient Global Reliability Analysis for Nonlinear Implicit Performance Functions," *AIAA Journal*, vol. 46, no. 10, pp. 2459–2468, Oct. 2008, doi: 10.2514/1.34321.

[32] T. H. Lee and J. J. Jung, "A sampling technique enhancing accuracy and efficiency of metamodel-based RBDO: Constraint boundary sampling," *Computers & Structures*, vol. 86, no. 13, pp. 1463–1476, 2008, doi: https://doi.org/10.1016/j.compstruc.2007.05.023.

[33] B. Echard, N. Gayton, and M. Lemaire, "AK-MCS: An active learning reliability method combining Kriging and Monte Carlo Simulation," *Structural Safety*, vol. 33, no. 2, pp. 145–154, 2011, doi: https://doi.org/10.1016/j.strusafe.2011.01.002.

[34] Z. Wang and P. Wang, "A Maximum Confidence Enhancement Based Sequential Sampling Scheme for Simulation-Based Design," *Journal of Mechanical Design*, vol. 136, no. 2, Dec. 2013, doi: 10.1115/1.4026033.

[35] Xu, Y., Renteria, A., and Wang, P., Adaptive Surrogate Models with Partially Observed Information, Reliability Engineering & Systems Safety, 2022. https://doi.org/10.1016/j.ress.2022.108566

[36] Dong, W., Moan, T., & Gao, Z. (2012). Fatigue reliability analysis of the jacket support structure for offshore wind turbine considering the effect of corrosion and inspection. Reliability Engineering & System Safety, 106, 11-27.

[37] Xie, C., Li, G., & Wei, F. (2018). An integrated QMU approach to structural reliability assessment based on evidence theory and kriging model with adaptive sampling. Reliability Engineering & System Safety, 171, 112-122.

[38] Feng, D. C., Xie, S. C., Li, Y., & Jin, L. (2021). Time-dependent reliability-based redundancy assessment of deteriorated RC structures against progressive collapse considering corrosion effect. Structural Safety, 89, 102061.

[39] Ma, Y., Wang, L., Zhang, J., Xiang, Y., Peng, T., & Liu, Y. (2015). Hybrid uncertainty quantification for probabilistic corrosion damage prediction for aging RC bridges. Journal of Materials in Civil Engineering, 27(4), 04014152.

[40] Heidary, R., & Groth, K. M. (2021). A hybrid population-based degradation model for pipeline pitting corrosion. Reliability Engineering & System Safety, 214, 107740.

[41] Sarkar, S., Warner, J. E., Aquino, W., & Grigoriu, M. D. (2014). Stochastic reduced order models for uncertainty quantification of intergranular corrosion rates. Corrosion Science, 80, 257-268.

[42] Sun, W., Wang, L., Wu, T., & Liu, G. (2014). An arbitrary Lagrangian–Eulerian model for modelling the time-dependent evolution of crevice corrosion. Corrosion Science, 78, 233-243.

[43] Sun, H., Wu, X., & Han, E. H. (2009). Effects of temperature on the protective property, structure and composition of the oxide film on Alloy 625. Corrosion Science, 51(11), 2565-2572.

[44] Sun, H., Wu, X., & Han, E. H. (2009). Effects of temperature on the oxide film properties of 304 stainless steel in high temperature lithium borate buffer solution. Corrosion Science, 51(12), 2840-2847.

[45] Wang, J., Wang, J., & Han, E. H. (2016). Influence of conductivity on corrosion behavior of 304 stainless steel in high temperature aqueous environment. Journal of Materials Science & Technology, 32(4), 333-340.

[46] Heppner, K., Evitts, R., & Postlethwaite, J. (2004). Effect of the Crevice Gap on the Initiation of Crevice Corrosion in Passive Metals. Corrosion. 60. 10.5006/1.3287850.

[47] Li, N., Zhang, W., Xu, H., Cai, Y., & Yan, X. (2022). Corrosion Behavior and Mechanical Properties of 30CrMnSiA High-Strength Steel under an Indoor Accelerated Harsh Marine Atmospheric Environment. Materials, 15(2), 629.

[48] Benjamin, I. (2021). Effects of Corrosion on Mechanical Properties of Reinforcing Steel Residual Flexural Strength. Sch Int J Chem Mater Sci, 4(6), 158-173.

[49] Fayomi, J., Popoola, A. P. I., Popoola, O. M., & Fayomi, O. S. I. (2021). The Appraisal of the thermal properties, electrical response, and corrosion resistance performance of AA8011 reinforced Nano Si3N4 for automobile application. Journal of Alloys and Compounds, 850, 156679.

[50] Echard, B., Gayton, N., & Lemaire, M. (2011). AK-MCS: an active learning reliability method combining Kriging and Monte Carlo simulation. Structural Safety, 33(2), 145-154.

[51] Hu, C., Youn, B. D., & Wang, P. (2019). Reliability-Based Design Optimization. In Engineering Design under Uncertainty and Health Prognostics (pp. 187-231). Springer, Cham.